Orbital Steering in the Catalytic Power of Enzymes: Small Structural Changes with Large Catalytic Consequences

Andrew D. Mesecar, Barry L. Stoddard, Daniel E. Koshland Jr.

Small structural perturbations in the enzyme isocitrate dehydrogenase (IDH) were made in order to evaluate the contribution of precise substrate alignment to the catalytic power of an enzyme. The reaction trajectory of IDH was modified (i) after the adenine moiety of nicotinamide adenine dinucleotide phosphate was changed to hypoxanthine (the 6-amino was changed to 6-hydroxyl), and (ii) by replacing Mg^{2+}, which has six coordinating ligands, with Ca^{2+}, which has eight coordinating ligands. Both changes make large (10^{-3} to 10^{-5}) changes in the reaction velocity but only small changes in the orientation of the substrates (both distance and angle) as revealed by cryocrystallographic trapping of active IDH complexes. The results provide evidence that orbital overlap produced by optimal orientation of reacting orbitals plays a major quantitative role in the catalytic power of enzymes.

Hypotheses analyzing and quantifying the factors that contribute to catalytic power have been proposed (*1–4*), but definitive experimental work supporting these hypotheses has been scant. Present-day developments in x-ray crystallography, such as time-resolved Laue and cryotrapping, localized mutagenesis, and molecular orbital calculations, provide opportunities to find correlations between theory and experiment. We have applied these new methods to make changes in the enzyme isocitrate dehydrogenase (IDH), which performs a well-known reaction (5) (Eq. 1),

$$\text{Isocitrate} + \text{NADP} \xrightarrow{Mg^{2+}} \text{oxalosuccinate} \xrightarrow{Mg^{2+}} \alpha\text{-ketoglutarate} + \text{NADPH} + CO_2 \quad (1)$$

has a known three-dimensional structure (6), has a well-developed kinetic mechanism (7), and has transient intermediates whose structures have been observed by time-resolved x-ray crystallography (8). We have perturbed the reaction trajectory of the enzyme in several ways to test whether small changes in the trajectory could have large effects on the catalytic efficiency (Fig. 1).

The first steady-state IDH reaction studied under catalytic turnover was that of the nicotinamide hypoxanthine dinucleotide (NHDP) complex, IDH-isocitrate-Mg^{2+}-NHDP. The reaction involved alteration of one of the substrates, nicotinamide adenine dinucleotide phosphate (NADP), that is modified at a position distant from the catalytic reaction center (Fig. 2). The second complex studied, IDH-isocitrate-Ca^{2+}-NADP, involved substitution of the normal divalent metal (Mg^{2+}), which is in a position near to the trajectory of the reacting groups but not on the path of hydride transfer, with Ca^{2+}. The structures of both of these active Michaelis complexes were solved with cryocrystallographic trapping methods, and these structures were compared to that of a complex of a Y160F mutant, IDH-isocitrate-Mg^{2+}-NADP, which has been solved by time-resolved x-ray crystallography (8). We define these three complexes as the Mg^{2+}-NHDP, Ca^{2+}-NADP, and Mg^{2+}-NADP quaternary complexes. The small structural changes observed for the aforementioned complexes are shown to be correlated to the large reductions in their catalytic rates.

Small trajectory changes via substrate modification. The first perturbation in the hydride transfer trajectory of IDH was made by replacing the NH_2 group at the 6 position of the normal substrate NADP with an OH group producing NHDP (Fig. 2). The 6-OH group of the hypoxanthine shown undergoes enol-keto tautomerization and is largely in the 6-keto form. This substitution occurs at a position that is >12 Å and 21 bond lengths away from the hydride that is transferred and has no effect on the $\Delta G°$ of the reaction. The data from kinetic studies with NHDP as a substrate show that such a substitution results in a dramatic decrease in the velocity of the reaction as reflected by the ratio of the turnover numbers for the complexes where $k_{cat,NHDP}/k_{cat,NADP} = 3.8 \times 10^{-5}$ (Table 1). In addition, there is also a large decrease in the second-order rate constant (k_{cat}/K_M), where the ratio of $(k_{cat,NHDP}/K_{M,NHDP})/(k_{cat,NADP}/K_{M,NADP})$ is 8×10^{-7}.

In order to show that such decreases in the reaction velocity are not due to decreases in the binding energy of the substrate, protein residues that are directly involved in binding NADP were mutated site specifically. Mutation of Lys^{344} to Met and Tyr^{345} to Phe, residues involved in binding NADP through its 2′ phosphate (Figs. 3 and 4), increases the K_M values for NADP to 390 and 750 μM respectively, values comparable to that of NHDP. However, the catalytic rates remain unchanged at 85 sec^{-1}. Such results indicate that a decrease in binding energy for the substrate is not the reason for the decrease in the catalytic rate in the case of NHDP, and that the orientation (distance and angle) of NHDP is a major factor in the decreased catalytic rate.

To correlate directly the reduction in the catalytic rate with structural perturbations, we used cryocrystallography (9) to trap active IDH in an intermediate state prior to hydride transfer. The fully active quaternary complex, Mg^{2+}-NHDP, diffracts to high resolution (1.9 Å) under cryogenic conditions. The phosphate backbone, the ribose, nicotinamide, hypoxanthine, and adenine rings of the cofactor, as well as isocitrate and metal, have observable and well-formed crystallographic electron densities (Fig. 3A and Table 2). The resulting complex provides distances and angles for the hydride transfer trajectory (Table 3).

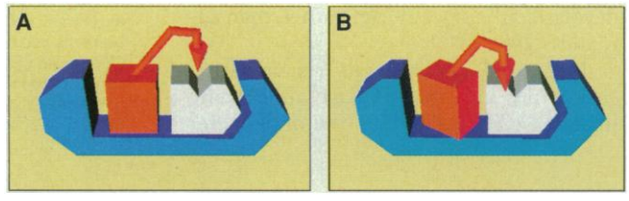

Fig. 1. Orbital steering in enzyme-catalyzed reactions can lead (**A**) to properly aligned substrates by maximizing bonding orbital overlaps and minimizing antibonding orbital overlaps or can lead (**B**) to improperly aligned substrates if the reaction coordinate trajectory is perturbed by modification.

A. D. Mesecar and D. E. Koshland Jr. are in the Department of Molecular and Cell Biology, Stanley Hall, University of California, Berkeley, CA 94720, and Center for Advanced Materials, Lawrence Berkeley National Laboratory, Berkeley, CA, USA. B. L. Stoddard is at the Division of Basic Sciences, Program in Structural Biology, Fred Hutchinson Cancer Research Center, 1124 Columbia Street A3-023, Seattle, WA 98104, USA.

The structure of the active quaternary Mg^{2+}-NHDP complex (Fig. 4) was compared to the active Mg^{2+}-NADP and Ca^{2+}-NADP quaternary complexes as well as to the binary IDH-NADP complex (*8*, *10*). The modification of the adenine ring in NADP to a hypoxanthine ring in NHDP causes the nucleotide to rotate by approximately 25 degrees about a rotation axis between the N7 and N9 nitrogens of the purine ring. The rotation caused a displacement of the altered atoms (N1 and O6) by 1.1 and 1.3 Å, respectively. The rotation and movement of the nucleotide was propagated along the entire phosphate backbone of the cofactor as a small translation, with a root-mean-square (rms) deviation of all atoms of approximately 0.8 Å. As a result, the ribose sugar ring that adjoins the nicotinamide moiety was rotated slightly in its binding site although its previously identified interactions with protein atoms were preserved (Figs. 3 and 4). The small movement of this sugar ring in turn was propagated to the nicotinamide ring, which shifted by approximately 2.5 Å relative to its position in the Mg^{2+}-NADP complex (Fig. 4). This movement is mostly lateral (in the plane of the ring) and causes the distance of the hydride donor-acceptor pair to increase by 1.55 Å (a covalent carbon-carbon bond distance is 1.54 Å) and the angles of approach to deviate between 10° to 20° from the more in-line geometry observed for the NADP structures (Table 3).

Trajectory perturbations triggered by metal coordination. To demonstrate further how small perturbations in the hydride transfer trajectory can lead to large decreases in catalytic rate, we took advantage of the preferred coordination number of divalent metals for ligands (*11*) and substituted Ca^{2+} for Mg^{2+} in the reaction. Magnesium and calcium are both considered to be "hard" Lewis acids, but magnesium prefers to coordinate to six ligands in protein structures, and calcium prefers to coordinate to seven or eight ligands (*11*). Substituting Ca^{2+} for Mg^{2+} in the IDH reaction lowers the enzymatic rate by a factor of approximately 2.5×10^{-3} and does not significantly alter the relative binding afffinities of the substrates or metals for the active site (Table 1). The very low catalytic activity of the Ca^{2+}-NADP enzyme complex allowed its three-dimensional structure to be solved by cryocrystallography.

As with the Mg^{2+}-NHDP quaternary complex, the crystals of the calcium complex diffracted to 1.9 Å resolution, and the electron density for the cofactor, isocitrate, and Ca^{2+} is clearly observable and interpretable (Fig. 3B). The structure of the calcium complex reveals an even smaller but detectable effect on the orientation (distance and angle) of the nicotinamide ring at the active site in comparison with the Mg-NADP quaternary complex structure (Fig. 4). The six-coordinate geometry of magnesium, in which the oxygen ligands are in a nearly optimal octahedral geometry in both the Mg^{2+}-NADP and Mg^{2+}-NHDP complexes, is illustrated for the Mg^{2+}-NHDP complex (Fig. 5A). The coordination positions of Mg^{2+} are normally occupied by two oxygens from isocitrate, two

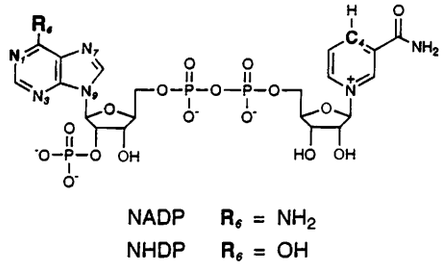

Fig. 2. Schematic illustration of NADP and NHDP.

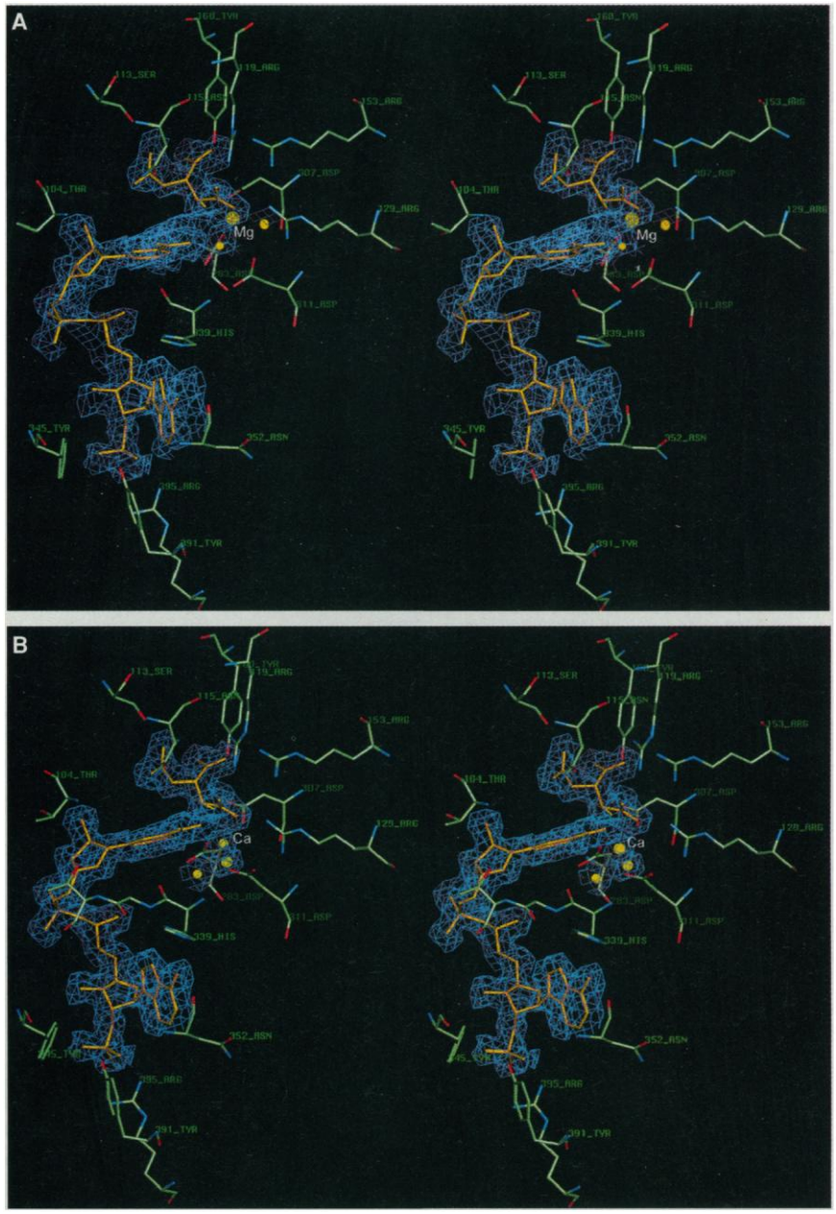

Fig. 3. Electron density difference maps for the bound, cryotrapped quaternary complexes at 1.9 Å resolution, contoured at 2.0 σ. (**A**) Final simulated annealing omit F_o-F_c map of NHDP, isocitrate, and Mg^{2+} calculated in X-PLOR (*22*) with coordinates for wild-type IDH after final positional refinement for the phase and map calculation. Coordinates for the bound cofactor and substrate were not included in the calculation. Only features of density within 2.0 Å of the cofactor and substrate atoms (yellow) are displayed for clarity. The unlabeled yellow spheres correspond to the metal-bound waters. (**B**) Difference Fourier map calculated in an identical manner for a cryotrapped complex of NADP, isocitrate, and Ca^{2+}.

oxygens from the protein amino acid side chains of Asp 283 and Asp 307, and two oxygens from water molecules that are well ordered (low thermal factors) and clearly observable in the electron density (Fig. 3). Substitution of Ca^{2+} for Mg^{2+} causes an inner coordination sphere rearrangement of the two water molecules and increases the coordination number of Ca^{2+} to 8 with an approximate pentagonal bipyramid geometry (Fig. 5B), similar to Ca^{2+} coordination in proteinase K and thermitase (*12*). The movement of the waters into new coordination positions occurs through a process in which calcium picks up two additional ligands from Asp^{311} by forming a direct bidentate coordination with the side chain carboxylate oxygens that are hydrogen-bonded to the water molecules in the Mg^{2+} ligation sphere (Fig. 5A). The rearrangement causes calcium to move approximately 1.4 Å from the position normally occupied by Mg^{2+} and in a direction that allows one of the calcium-bound water molecules to form a hydrogen bond with the backbone carbonyl of Thr^{338}. The movement also places calcium above the plane formed by Mg^{2+}, and the oxygens of the α-carboxylate and β hydroxy of isocitrate, reminiscent of iron moving out of the plane of the heme upon deoxygenation in hemoglobin (*13*). The small yet tangible movement of calcium results in an adjustment of isocitrate, NADP, and the side chains of the aspartate residues, thereby decreasing the distance between the hydride donor-acceptor pair by 0.55 Å and altering the attacking and dihedral angles (Table 3).

To test whether the velocity changes observed for the complexes studied were a result of the coordination geometry and not attributable to a difference in the atomic radii of the metal (the radius of Mg^{2+} is 0.65 Å, whereas the radius of Ca^{2+} is 0.99 Å), we determined the kinetics of the Cd^{2+}-catalyzed reaction. Cadmium has practically the same radius as Ca^{2+} (0.97 Å compared with 0.99 Å), but Cd^{2+} prefers a six-coordinate, octahedral ligand geometry similar to that of Mg^{2+}, whereas Ca^{2+} does not (*11*). The Cd^{2+}-catalyzed rate of the enzyme is equal to the fast rate of the small, Mg^{2+}-catalyzed enzyme instead of the very slow rate of the similarly sized and differently coordinated Ca^{2+} (Table 1). The homologous pig heart enzyme is also not activated by Ca^{2+} and is twice as active in the presence of Cd^{2+} than in the presence of Mg^{2+} (*14*). Structural evidence for six coordinate octahedral symmetry of the Cd^{2+} and Mg^{2+} ligation sphere was obtained by ^{113}Cd and ^{25}Mg NMR studies (*15*).

These results emphasize the importance of small perturbations in making major changes in the catalytic power of enzymes and organic reactions and supports the theory of orbital steering (*2*),

Table 1. Steady-state kinetic parameters for IDH complexes. Isocitrate dehydrogenase kinetics were measured at 25°C and in 100 mM tris buffer, pH = 7.8, by monitoring the production of either NADPH or NHDPH. The molar extinction coefficients used for both NADPH and NHDPH were 6220 M^{-1} cm^{-1}. Reaction times for the Mg^{2+} and Cd^{2+} NADP complexes were complete in under 2 min, whereas reactions with NHDP and Ca^{2+} were monitored for at least 1 hour in order to measure the slow kinetic rates. The concentration of enzyme was kept low in order to maintain a steady-state concentration of reactants and to treat total ligand concentrations as free. Michaelis constants and k_{cat} values were obtained by fitting initial velocity data to the Michaelis-Menten equation.

IDH-isocitrate complex	Cation radius (Å)	Redox potential (mV)	k_{cat} (sec^{-1})	K_M or K_A (μM)	K_I* (μM)	k_{cat} ratio‡
Mg^{2+}-NADP	0.65	−320	80.1	14.4		1
Mg^{2+}-NHDP	0.65	−320	0.00305	657	403	3.8×10^{-5}
Ca^{2+}-NADP	0.99	−320	<0.2†	6	2.7	$<2.5 \times 10^{-3}$
Cd^{2+}-NADP	0.97	−320	79	3.5		1

*The extremely slow rates of IDH catalysis with either NHDP or Ca^{2+} allows the determination of their inhibition constants (K_I). Both NHDP and Ca^{2+} are linear competitive inhibitors. †After exhaustive attempts to remove contaminating metals from substrates, buffers, water, and the enzyme with Chelex-100 and Bio-Rex chelating resins and disks, background activity in the absence of any added metal was measured at 0.1 sec^{-1}. With the use of the K_M and k_{cat} values for Mg^{2+} activation, a contaminating metal concentration of 0.02 μM Mg^{2+} or roughly 0.5 ppb is calculated as a possible source for the activity. This made the measurement of the Ca^{2+} rate an upper limit of 0.2 sec^{-1} because the rates were scattered around that of the background ±50% in the Ca^{2+} concentration range of 0 to 50 μM. ‡Relative to the wild-type Mg-isocitrate–NADP complex.

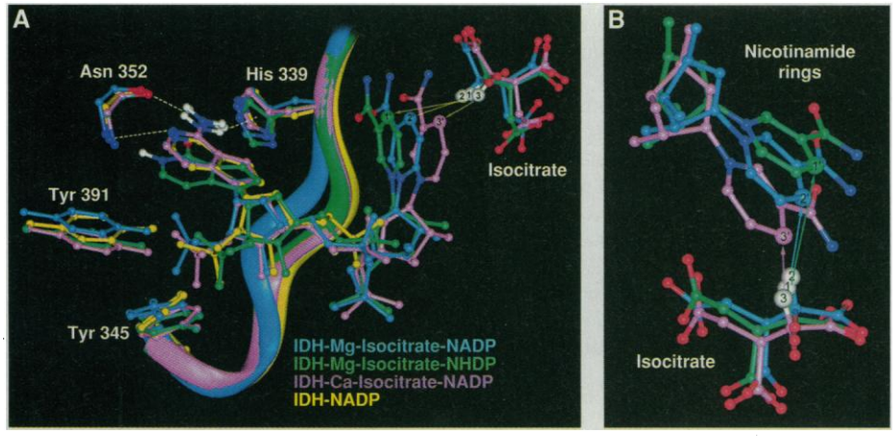

Fig. 4. Superpositions (*23*) of various IDH complexes, including isocitrate-Mg^{2+}-NHDP (green) and isocitrate-Ca^{2+}-NADP (pink), Y160F-IDH-isocitrate-Mg^{2+}-NADP (blue) solved by time-resolved Laue crystallography (*8*), and IDH-NADP (yellow) (*10*). In (**A**) the rotation of the adenine ring, which occurs on mutation to a hypoxanthine derivative, is evident and differs from both the Mg^{2+}- and Ca^{2+}-NADP structures. The driving force behind this movement appears to be the formation of a pair of interactions between the O_6 carbonyl oxygen and two separate protein atoms in the nucleotide binding cleft at 3.0 Å to the ε-nitrogen of His^{339} and 3.3 Å to the backbone nitrogen of Asn^{352}. These interactions are aligned in the plane of the electron pairs of the sp^2-hybridized O_6 oxygen when the ring is rotated, as described above, with bond angles through the oxygen of 130° and 95°, respectively. In addition, the N1 nitrogen of hypoxanthine ring is in contact with the side chain oxygens of Asn^{352} and Asp^{392}. The hypoxanthine nucleotide ring is hindered from rotating further in the pocket to completely optimize these interactions by the packing of protein atoms against both faces of the purine ring, and by the electrostatic interactions between the ribose phosphate and Arg^{395} and $Arg^{292'}$, which serve to further anchor the nucleotide. However, the distances between that same phosphate and two neighboring tyrosines that bind NADP (345 and 391) have increased by approximately 1.4 Å each, whereas the contacts to the arginine residues are preserved. These changes in distance presumably contribute to the decrease in the binding affinity of this compound as compared to NADP. Backbone movement of residues 340 to 344 (ribbon representation), observed in the Laue structure, is most likely due to the room temperature dynamics of the protein under steady-state turnover (*8*). (**B**) An expanded view of the nicotinamide rings and isocitrate, as well as the hydride transfer paths (1 to 1′, 2 to 2′, 3 to 3′). The nicotinamide ring for the NADP in the binary IDH-NADP complex is not observable in the electron density (*10*). Placing the hydride donor atom (C2 of isocitrate) closer to its acceptor atom (C4 of the nicotinamide ring) does not accelerate the rate of the reaction; it actually decreases the rate of the reaction, indicating that orientation (angle) makes a major contribution to the catalytic rate.

which postulated that a major factor in the catalytic power of an enzyme is that it arranges the trajectory so that the balance between maximizing the overlaps of attractive (bonding) orbitals and minimizing the overlaps of repulsive (nonbonding) orbitals is optimized. These effects on the reaction of a hydride ion, one of the atoms that might be expected to be less susceptible to orientation effects, suggest that larger atoms may show even larger catalytic effects. Of course, the contribution of orbital steering to the enormous catalytic power of any one enzyme will vary with, and depend on, both the particular reaction type (condensation versus hydrolysis versus decarboxylation) and on the particular enzyme (isocitrate dehydrogenase versus alcohol dehydrogenase versus hydroxysteroid dehydrogenase, and the like). Thus, in many ways the hydride transfer reaction is the toughest test of the orbital steering concept and these results support the original theoretical deduction. Incidentally, in relation to the proposition that the closeness of approach of the reacting atoms is the only determining factor in the reactivity rate (3), the closeness is in the order Ca^{2+}-NADP > Mg^{2+}-NADP > Mg^{2+}-NHDP unlike the catalytic rates that are in the order Mg^{2+}-NADP > Ca^{2+}-NADP > Mg^{2+}-NHDP. Moreover, analyses of the geometrical relations in the hydride transfer trajectories of the three IDH complexes studied (Table 3) indicates that the hydride transfer angle (N-C4–H) is <180° and not on-line at 180°. Attack angles in model hydride transfer reactions and in dehydrogenase reactions have been calculated by various computational methods and in most cases the N-C4–H angle was calculated to be <180° (16) as is observed in the above structures of IDH. Analyses of the structures of other hydride transferring enzymes, either modeled ternary complex structures from their experimental binary complex structures or from inhibitor or product ternary complexes, also support our data that hydride transfer occurs at angles different from 180° and at distances between 3 to 5 Å (17).

If it is argued that the major factor in the decrease in reactivity (10^4) of NHDP is the increased distance relative to NADP, then it would have to be argued that the change of reactivity of Ca^{2+} versus Mg^{2+} would have to be a very large increase in reactivity due to a closer distance and an extremely large decrease due to poor orientation. It is more reasonable to assume that both the orientational overlap and the distance overlap play major roles in both examples but with a more clear-cut quantitative assignment in the metal ion case because the distance is closer but the rate is decreased.

These results in an active enzyme give experimental support to the hypothesis that the catalytic power of enzymes derives in large part from the ability of the enzyme to direct a trajectory that maxi-

Table 2. Data processing and refinement statistics. Crystals of wild-type IDH were grown as described (6) and transferred to a mother liquor consisting of 40 percent saturated ammonium sulfate, buffered at pH 7.5 with 100 mM tris that was supplemented with the components of two separate soaks [(i) 100 mM isocitrate, 50 mM Mg^{2+}, 500 mM NHDP; (ii) 100 mM isocitrate, 50 mM Ca^{2+}, 500 mM NADP). The soaks each proceeded for 2 hours, and the crystals were then transferred stepwise to the same solutions, either A or B, further supplemented with 10, 20, and 30 percent glycerol, respectively, for 10 min each. The crystals were mounted in a rayon loop and directly flash-cooled in liquid nitrogen and were then transferred to a stream of dry nitrogen gas at −185°C for data collection (18). One crystal was used for each data set collected. All data were collected at beamline X12-C at Brookhaven National Laboratory, with a MAR phosphor image plate detector mounted on a Kappa-axis goniometer (Enraf-Nonius), which allows complete data sets to be collected. Data were processed and scaled with DENZO and SCALEPACK (19). Based on data processing and refinement, the space group and unit cell parameters are $P4_32_12$, with $a = b = 102.4$ Å and $c = 150.6$ Å, as previously reported for IDH flash-cooled crystals (20). The *a* and *b* axes shrink by nearly 3 percent relative to room temperature, and a molecular replacement search was used to position the models (21), which were then refined with X-PLOR (22). All data to 1.9 Å resolution were included in the final refinement. After refinement of the protein, the substrate, divalent cation, and nicotinamide nucleotide cofactors were manually built into $(F_o\text{-}F_c)\alpha_{calc}$ difference Fourier maps using QUANTA (Molecular Simulations), and refinements were continued. The final working and free *R* factors for each complex were 0.188 and 0.220 for the Mg^{2+}-NHDP complex and 0.191 and 0.215 for the Ca^{2+}-NADP complex.

	NHDP-isocitrate-Mg^{2+} (wild type)	NADP-isocitrate-Ca^{2+} (wild type)	NADP-isocitrate-Mg^{2+} (Y160F) (8)
Reaction trapping	Flash-cooling	Flash-cooling	Steady-state
Data collection	Monochromatic	Monochromatic	Polychromatic
Wavelength (Å)	1.40	1.40	0.7-1.5
Resolution (Å)	1.9	1.9	2.5
Reflections			
Total (*n*)	198,342	183,903	310,414
Unique (*n*)	62,143	63,007	17,943
Completeness (%)	97.2 (50-1.9 Å)	98.6 (50-1.9 Å)	83.0 (4-2.5 Å)
R_{sym}*	0.060	0.059	0.084
$R_{refinement}$†	.188	.191	.172
R_{free}‡	.220	.215	.246
Root-mean-square deviation			
Bond distance (Å)	0.013	0.014	0.016
Bond angle (Å)	2.8	2.7	3.2

*R_{sym} = Initial overall *R* factor (on intensities) between all symmetry-related reflections in the final merged data set. $R = \Sigma_j (I_1(j) - I_2(j))/\Sigma_j (I(j))$; †$R_{refinement} = \Sigma_j |(F_o(j) - F_c(j))|/\Sigma_j (F_o(j))$; ‡$R_{free}$ is the overall agreement between measured and calculated structure factor amplitudes as defined in (22), monitored for a random sampling of 5 percent of the total reflections that were withheld from all stages of refinement.

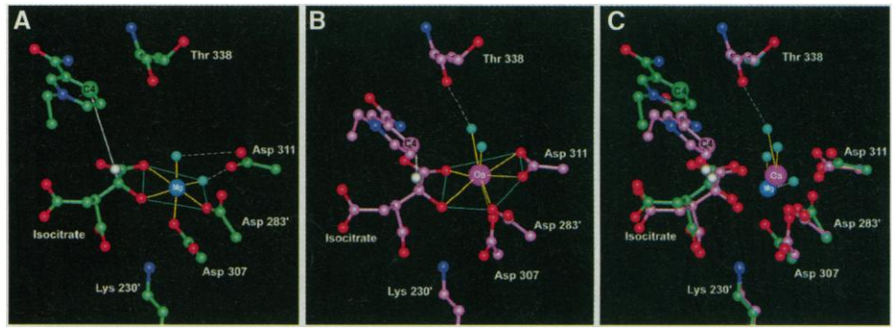

Fig. 5. Coordination geometry of Mg^{2+} and Ca^{2+} in the active IDH quaternary complexes (**A**) IDH-isocitrate-Mg^{2+}-NHDP and (**B**) IDH-isocitrate-Ca^{2+}-NADP. Mg^{2+} (dark blue sphere) is shown coordinated (yellow lines) in an octahedral arrangement to its six first-sphere ligands, isocitrate, $Asp^{283'}$, Asp^{307}, and water (light blue spheres). Asp^{311} hydrogen bonds to the two water molecules. Ca^{2+} (dark pink sphere) is shown coordinated in an approximate pentagonal bipyramid (blue lines) geometry to its eight first-sphere ligands, isocitrate, $Asp^{283'}$, Asp^{307}, Asp^{311}, and water. Thr^{338} forms a hydrogen bond with one of the water molecules that is 2.32 Å away. (**C**) A superposition (23) of the two complexes illustrates the small movements that occur at the active site that lead to a large decrease in catalytic activity between the two complexes.

Table 3. Distances and angular geometries of hydride transfer in the IDH-catalyzed reaction. Two sets of trajectory geometries, including both distances (Å) and angles (°), are defined for the IDH reaction trajectory.

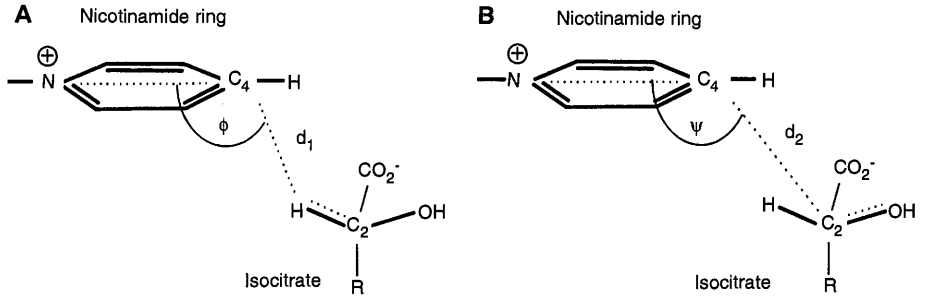

IDH complex	A, set 1 (d_1) C_4–H (Å)	A, set 1 (ϕ) N-C_4–H (°)	A, set 1 Dihedral* N-C_4–H-C_2 (°)	B, set 2 (d_2) C_4–C_2 (Å)	B, set 2 (ψ) N-C_4–C_2 (°)	B, set 2 Dihedral* N-C_4–C_2-$O_{(OH)}$ (°)	Reaction rate† (sec^{-1})
Mg-NADP‡	2.70	123	159	3.74	129	−75	0.3
Mg-NHDP	4.37	104	144	5.29	110	−85	0.0030
Ca-NADP	2.14	141	131	3.19	145	−115	<0.2

*The dihedral angles are represented by the dashed lines. †The wild-type Mg-NADP complex reaction rate is 85 sec^{-1}. ‡From the structure of the Y160F-IDH solved by time-resolved Laue x-ray crystallography (*8*).

mizes the orbital steering contribution to catalysis. The results are a forerunner of the more accurate calculations and experiments that we can expect from applying similar tools to evaluating the factors involved in the catalytic power of enzymes and the design of new catalysts. Moreover, these results suggest that small structural changes may be important in biological and chemical processes such as allosterism, signal transduction, molecular recognition, and biocatalysis (enzymes, ribozymes, and catalytic antibodies). Consideration of orbital steering factors in these processes may aid in their being understood and may prove useful for increasing the catalytic power of suboptimal catalysts, changing specificity of reactions for synthesis of novel compounds and pharmaceuticals, and for boosting the biodegradative potentials of organisms.

REFERENCES AND NOTES

1. T. C. Bruice and V. K. Pandit, *J. Am. Chem. Soc.* **82**, 5858 (1960); T. C. Bruice, *Annu. Rev. Biochem.* **45**, 331 (1976).
2. D. E. Koshland Jr., *J. Theoret. Biol.* **2**, 75 (1962); ——— and K. E. Neet, *Annu. Rev. Biochem.* **37**, 359 (1968); D. A. Storm and D. E. Koshland Jr., *Proc. Natl. Acad. Sci. U.S.A.* **66**, 445 (1970); A. Dafforn and D. E. Koshland, Jr., *ibid.* **68**, 2463 (1971).
3. M. I. Page and W. P. Jencks, *J. Am. Chem. Soc.* **94**, 8828 (1972); S. Schreiner, W. N. Lipscomb, D. A. Kleier, *ibid.* **98**, 4770 (1976); F. M. Menger, *Acc. Chem. Res.* **18**, 128 (1985); K. A. Brown and J. Kraut, *Farraday Disc.* **93**, 217 (1992); W. M. Kati, S. A. Ackerson, R. Wolfenden, *Biochemistry* **31**, 7356 (1992); D. D. Hackney, in *The Enzymes*, P. D. Boyer *et al.*, Eds. (Academic Press, New York, ed. 3, 1990), pp. 1–36; D. W. Huhta *et al.*, *Acta Chem. Scand.* (1992), p. 778; F. M. Menger, *Acc. Chem. Res.* **26**, 206 (1993).
4. A. Warshel, *Computer Modeling of Chemical Reaction in Enzymes and Solution* (Wiley, New York, 1991).
5. L. Stryer, *Biochemistry* (Freeman, New York, ed. 3, 1988), p. 375.
6. J. H. Hurley *et al.*, *Proc. Natl. Acad. Sci. U.S.A.* **86**, 8635 (1989); J. H. Hurley, A. M. Dean, J. L. Sohl, D. E. Koshland Jr., R. M. Stroud, *Science* **249**, 1012 (1990); B. L. Stoddard and D. E. Koshland Jr., *Biochemistry* **32**, 9317 (1993).
7. D. B. Northrop and W. W. Cleland, *J. Biol. Chem.* **249**, 2928 (1974); A. M. Dean and D. E. Koshland Jr., *Biochemistry* **32**, 9302 (1993).
8. J. M. Bolduc *et al.*, *Science* **268**, 1312 (1995); B. L. Stoddard, A. Dean, P. A. Bash, *Nature Struct. Biol.* **3**, 590 (1996).
9. D. W. Christianson and W. N. Lipscomb, *Proc. Natl. Acad. Sci. U.S.A.* **83**, 7568 (1986); H. D. Bartunik, L. J. Bartunik, H. Viemann, *Philos. Trans. R. Soc. London Ser. A* **340**, 209 (1992); X. Ding, B. F. Rasmussen, G. A. Petsko, D. Ringe, *Biochemistry* **33**, 9285 (1994); I. Schlichting, J. Berendzin, G. N. Phillips, R. M. Sweet, *Nature* **371**, 808 (1994).
10. J. H. Hurley, A. M. Dean, D. E. Koshland Jr., R. M. Stroud, *Biochemistry* **30**, 8671 (1991).
11. J. P. Glusker, *Adv. Prot. Chem.* **42**, 1 (1991); C. A. McPhalen, N. C. J. Strynadka, M. N. G. James, *ibid.*, p. 77.
12. J. Bajorath, W. Hinrichs, W. Sänger, *Nature* **337**, 481 (1989); P. Gros, A. V. Teplyakov, W. G. Hol, *Proteins* **12**, 63 (1992).
13. M. F. Perutz, *Mechanisms of Cooperativity and Allosteric Regulation in Proteins* (Cambridge Univ. Press, New York, 1990).
14. R. F. Colman, *J. Biol. Chem.* **247**, 215 (1972).
15. R. S. Ehrlich and R. F. Colman, *Biochemistry* **28**, 2058 (1989); *Biochim. Biophys. Acta* **1246**, 135 (1995).
16. M. C. A Donkersloot and H. M. Buck, *J. Am. Chem. Soc.* **103**, 6549, 6554 (1981); Y. D. Wu and K. N. Houk, *ibid.* **109**, 2226 (1987); R. Sustman, W. Sicking, G. E. Schulz, *Angew. Chem. Int. Ed. Engl.* **28**, 1023 (1989); M. J. Sherrod and F. M. Menger, *J. Am. Chem. Soc.* **111**, 2611 (1989); I. H. Williams, A. B. Miller, G. M. Maggiora, *ibid.* **112**, 530 (1990); P. L. Cummins and J. E. Gready, *J. Comp. Chem.* **11**, 791 (1990); M. J. Sherrod and F. M. Menger, *Tetrahedron Lett.* **31**, 459 (1990); N. Bodor, M. E. Brewster, J. J. Kaminski, *J. Mol. Struct. Theorchem.* **206**, 315 (1990); Y. D. Wu, K. N. Houk, *J. Am. Chem. Soc.* **113**, 2353 (1991); O. Almarsson and T. C. Bruice, *ibid.* **115**, 2125 (1993).
17. P. A. Karplus and G. E. Schulz, *J. Mol. Biol.* **210**, 163 (1989); C. Bystroff, S. J. Oatley, J. Kraut, *Biochemistry* **29**, 3263 (1990); M. A. McTigue, J. F. Davies II, B. T. Kaufman, J. Kraut, *ibid.* **31**, 7264 (1992); M. D. Hall and L. J. Banaszak, *J. Mol. Biol.* **232**, 213 (1993); M. A. McTigue, J. F. Davies II, B. T. Kaufman, J. Kraut, *Biochemistry* **32**, 6855 (1993); D. H. Harrison, K. M. Bohren, D. Ringe, G. A. Petsko, K. H. Gabbay, *ibid.* **33**, 2011 (1994); S. Ramaswamy, H. Eklund, B. V. Plapp, *ibid.*, p. 5230; N. Tanaka *et al.*, *Structure* **4**, 33 (1996); J. B. Thoden, P. A. Frey, H. M. Holden, *Protein Sci.* **5**, 2149 (1996); N. Tanaka *et al.*, *Biochemistry* **35**, 7715 (1996).
18. This strategy for data collection and for trapping reactive enzyme intermediate is advantageous because (i) the resolution is increased significantly (both data sets are measured to 1.9 Å resolution) and (ii), the structure of a complex that turns over very slowly at room temperature (such as NHDP in the active site of IDH) is physically trapped at the low temperature of data collection, allowing analysis of a transient population that displays dynamic movement and catalytic heterogeneity at higher temperatures.
19. Z. Otwinowski, *Proceedings of the CCP4 Study Weekend: Data Collection and Processing*, L. Sawyer, N. Isaacs, S. Bailey, Eds. (SERC Daresbury Laboratory, UK).
20. J. H. Hurley, R. Chen, A. M. Dean, *Biochemistry* **35**, 5670 (1996).
21. J. Naveza, *Acta Crystallogr. A* **50**, 157 (1994).
22. A. Brünger, X-PLOR, version 3.1 (Yale Univ. Press, New Haven, CT, 1992).
23. The structures of the bound complexes were compared by at least-squares superposition of alpha-carbons from the enzyme dimers by means of the protein design module of the program Quanta (Quanta96 X-ray Structure Analysis User's Reference, San Diego: Molecular Simulations, 1996).

24. Supported by NSF grant 04200 (D.E.K.), by a DOE fellowship (A.D.M.), NIH grant GM49857 (B.L.S.), and a grant from the Keck Foundation. Coordinates for the Ca^{2+}-NADP and Mg^{2+}-NHDP complexes have been submitted to the Brookhaven Protein Data Base with accession numbers 1AI2 and 1AI3 respectively; the code number for the coordinates for the Y160F Laue complex in the PDB is 1IDE.

9 December 1996; accepted 5 May 1997